Acta Mech 198, 171–190 (2008)
DOI 10.1007/s00707-007-0526-9
Printed in The Netherlands

Acta Mechanica

Circumferential wave in functionally graded piezoelectric cylindrical curved plates

Y. Jiangong[1], M. Qiujuan[2]

[1] School of Mechanical and Power Engineering, Henan Polytechnic University, Jiaozuo, P.R. China
[2] College of Water Conservancy and Hydroelectricity, Hebei University of Engineering, Handan, P.R. China

Received 4 July 2007; Accepted 11 October 2007; Published online 25 January 2008

Summary. Functionally graded piezoelectric material (FGPM), with a gradual change of the mechanical and electric properties, has large fields of application. Based on linear three-dimensional piezoelasticity, a Legendre orthogonal polynomial series expansion approach is used for determining the characteristics of circumferential waves in FGPM cylindrical curved plates. Our results from an FGPM cylindrical curved plate with a large ratio of radius to thickness are compared with an FGPM flat plate published earlier to confirm the accuracy and range of applicability of the computational program. Circumferential wave dispersion curves for FGPM and the corresponding FGM cylindrical curved plates are calculated and the effect of piezoelectricity is shown. The influence of the ratio of radius to thickness on the piezoelectric effect and electric potential distribution is discussed. The ratio has a significant influence on the electric potential distribution. Finally, the influence of the polarizing direction on the piezoelectric effect is illustrated. The phenomenon that piezoelectricity weakens the guided wave dispersion in the FGPM cylindrical plate is observed.

1 Introduction

To enhance the effect of piezoelectric materials (PEM), the concept of functionally graded piezoelectric material has been proposed and termed FGPM. Techniques for fabricating FGPM have been developed [1]. Zhu and Meng [2] and Wu et al. [3] have reported the development of FGPM actuators with gradation of compositions from high to low piezoelectric property and low to high dielectric property. Mahapatra et al. [4] had discussed the advantages of FGPM interdigital transducers (IDT) over the traditional IDT. The behavior of the wave mode selected directly affects the performance of the device. Thus, in the applications of FGPM to SAW devices, the study of wave propagation behavior in FGPM structures is of considerable importance.

In 1991, Liu and Tani [5], [6] proposed a hybrid numerical method for the characteristics and response of wave propagation in FGPM plates, where the FGPM layer is divided into a number of

Correspondence: Yu Jiangong, School of Mechanical and Power Engineering, Henan Polytechnic University, Jiaozuo, 454003, P.R. China
e-mail: yu@emails.bjut.edu.cn

inhomogeneous thin layers and the Fourier transformation method was employed. Recently, Lefebvre et al. [7] used the Legendre polynomial approach for acoustic wave propagation in continuous FGPM plates. Han et al. [8] used linearly inhomogeneous elements to analyze the wave characteristics in FGPM cylinders. Afterwards, Liu et al. [9] proposed quadratic inhomogeneous elements for the dispersion of waves and characteristics waves in FGPM plates. Chakraborty et al. [10] formulated a set of finite elements to analyze wave propagation through FGPM plates when subjected to mechanical, and thermal loading or piezoelectric actuation, where the material properties are allowed to vary both in length and in thickness direction. Chakraborty et al. [11] used the spectral element method characterizing the wave propagation in FGPM plates by the thin-layer model, and modeled an ultrasonic transducer composed of FGPM. Li et al. [12] and Liu et al. [13] studied the propagation of a love wave in the FGPM structure by the WKB method. Du et al. [14] gave the Love wave analytical solutions of the dispersion relations. Based on higher-order shear deformation theory, Mahapatra et al. [4] used the spectral element method investigating the Lamb wave characteristics in FGPM plates, and pointed out that there was the reduced dispersion of the Lamb wave modes in FGPM plates.

Hollow cylinders, as common engineering structures, have also received a lot of attention to the problem of wave propagation. Much work has been reported on the axial propagation of guided waves in hollow cylinders. Different aspects of the circumferential direction wave propagation along one or multiple curved surfaces have been analyzed by Grace and Goodman [15], Qu and Berthelot [16], Cerv [17], Liu and Qu [18], [19], Valle et al. [20], He and Li [21] in an isotropic elastic material. Towfighi et al. [22] studied the circumferential direction wave propagation in an anisotropic elastic material using the Fourier series expansions method. Yu et al. [23] studied the circumferential direction wave propagation and the mode conversion by the end-reflection in an orthotropic cylindrical curved plate. Zhao and Rose [24] studied the circumferential SH wave in isotropic hollow cylinders. In addition, the surface acoustic wave ΣSAWΠ device on a hollow cylinder can provide high-performance sensors, and piezoelectric cylindrical curved plate transducers have received too much attention to be listed here.

The objective of this paper is to present the results of a circumferential wave in an FGPM cylindrical curved plate by the Legendre orthogonal polynomial series expansion method, which is developed by Lefebvre et al. [25] to solve the free-ultrasonic waves in multilayered plates. Results from an FGPM cylindrical curved plate with a large ratio of radius to thickness are compared with an FGPM flat plate published earlier to confirm the accuracy and range of applicability of the developed Mathematica program. Circumferential wave dispersion curves for FGPM and the corresponding FGM cylindrical curved plates are calculated and the effect of piezoelectricity is shown. The influence of the ratio of radius to thickness on the piezoelectric effect and electric potential distribution is discussed. Finally, the influence of the polarizing direction on the piezoelectric effect is illustrated. In this paper, the open circuit surface is assumed.

2 Mathematics and formulation of the problem

Based on linear three-dimensional piezoelasticity, consider an anisotropic FGPM hollow cylinder. In the cylindrical coordinate system (θ, z, r), a, b, h are the inner and outer radii and the thickness, respectively.

The linear constitutive relations of an anisotropic cylindrical piezoelectric medium are

$$\begin{Bmatrix} T_{\theta\theta} \\ T_{zz} \\ T_{rr} \\ T_{rz} \\ T_{r\theta} \\ T_{\theta z} \end{Bmatrix} = \begin{bmatrix} C_{11} & C_{12} & C_{13} & C_{14} & C_{15} & C_{16} \\ & C_{22} & C_{23} & C_{24} & C_{25} & C_{26} \\ & & C_{33} & C_{34} & C_{35} & C_{36} \\ & & & C_{44} & C_{45} & C_{46} \\ & \text{symmetry} & & & C_{55} & C_{56} \\ & & & & & C_{66} \end{bmatrix} \begin{Bmatrix} \varepsilon_{\theta\theta} \\ \varepsilon_{zz} \\ \varepsilon_{rr} \\ 2\varepsilon_{rz} \\ 2\varepsilon_{r\theta} \\ 2\varepsilon_{\theta z} \end{Bmatrix} - \begin{bmatrix} e_{11} & e_{21} & e_{31} \\ e_{12} & e_{22} & e_{32} \\ e_{13} & e_{23} & e_{33} \\ e_{14} & e_{24} & e_{34} \\ e_{15} & e_{25} & e_{35} \\ e_{16} & e_{26} & e_{36} \end{bmatrix} \begin{Bmatrix} E_\theta \\ E_z \\ E_r \end{Bmatrix}, \tag{1.1}$$

$$\begin{Bmatrix} D_\theta \\ D_z \\ D_r \end{Bmatrix} = \begin{bmatrix} e_{11} & e_{12} & e_{13} & e_{14} & e_{15} & e_{16} \\ e_{21} & e_{22} & e_{23} & e_{24} & e_{25} & e_{26} \\ e_{31} & e_{32} & e_{33} & e_{34} & e_{35} & e_{36} \end{bmatrix} \begin{Bmatrix} \varepsilon_{\theta\theta} \\ \varepsilon_{zz} \\ \varepsilon_{rr} \\ 2\varepsilon_{rz} \\ 2\varepsilon_{r\theta} \\ 2\varepsilon_{\theta z} \end{Bmatrix} + \begin{bmatrix} \in_{11} & \in_{12} & \in_{13} \\ & \in_{22} & \in_{23} \\ \text{symmetry} & & \in_{33} \end{bmatrix} \begin{Bmatrix} E_\theta \\ E_z \\ E_r \end{Bmatrix}. \tag{1.2}$$

Generalized geometric equations for cylindrical coordinates are

$$\begin{aligned} &\varepsilon_{\theta\theta} = \frac{1}{r}\frac{\partial u_\theta}{\partial \theta} + \frac{u_r}{r}, \quad \varepsilon_{zz} = \frac{\partial u_z}{\partial z}, \quad \varepsilon_{rr} = \frac{\partial u_r}{\partial r}, \\ &\varepsilon_{r\theta} = \frac{1}{2}\left(\frac{1}{r}\frac{\partial u_r}{\partial \theta} + \frac{\partial u_\theta}{\partial r} - \frac{u_\theta}{r}\right), \quad \varepsilon_{rz} = \frac{1}{2}\left(\frac{\partial u_r}{\partial z} + \frac{\partial u_z}{\partial r}\right), \quad \varepsilon_{\theta z} = \frac{1}{2}\left(\frac{\partial u_\theta}{\partial z} + \frac{\partial u_z}{r\partial \theta}\right), \\ &E_\theta = -\frac{1}{r}\frac{\partial \Phi}{\partial \theta}, \quad E_z = -\frac{\partial \Phi}{\partial z}, \quad E_r = -\frac{\partial \Phi}{\partial r}. \end{aligned} \tag{2}$$

And the field equations governing wave propagation are

$$\begin{aligned} &\frac{\partial T_{rr}}{\partial r} + \frac{1}{r}\frac{\partial T_{r\theta}}{\partial \theta} + \frac{\partial T_{rz}}{\partial z} + \frac{T_{rr} - T_{\theta\theta}}{r} = \rho\frac{\partial^2 u_r}{\partial t^2}, \\ &\frac{\partial T_{r\theta}}{\partial r} + \frac{1}{r}\frac{\partial T_{\theta\theta}}{\partial \theta} + \frac{\partial T_{\theta z}}{\partial z} + \frac{2T_{r\theta}}{r} = \rho\frac{\partial^2 u_\theta}{\partial t^2}, \\ &\frac{\partial T_{rz}}{\partial r} + \frac{1}{r}\frac{\partial T_{\theta z}}{\partial \theta} + \frac{\partial T_{zz}}{\partial z} + \frac{T_{rz}}{r} = \rho\frac{\partial^2 u_z}{\partial t^2}, \\ &\frac{\partial D_r}{\partial r} + \frac{1}{r}\frac{\partial D_\theta}{\partial \theta} + \frac{\partial D_z}{\partial z} + \frac{D_r}{r} = 0, \end{aligned} \tag{3}$$

where T_{ij} and ε_{ij} are the stress and strain tensors; Φ and D_i are the electric potential and electric displacement vector; C_{ij}, $\in_{ij}$ and e_{ij} are the elastic, dielectric and piezoelectric constants; and ρ is mass density.

Because the material properties of FGPM vary in the radial direction, the elastic, dielectric, piezoelectric constants and mass density of the medium are functions of the radius,

$$\begin{aligned} C(r) &= C^{(0)} + C^{(1)}\left(\frac{r}{h}\right)^1 + C^{(2)}\left(\frac{r}{h}\right)^2 + \cdots + C^{(L)}\left(\frac{r}{h}\right)^L, \\ e(r) &= e^{(0)} + e^{(1)}\left(\frac{r}{h}\right)^1 + e^{(2)}\left(\frac{r}{h}\right)^2 + \cdots + e^{(L)}\left(\frac{r}{h}\right)^L, \\ \in(r) &= \in^{(0)} + \in^{(1)}\left(\frac{r}{h}\right)^1 + \in^{(2)}\left(\frac{r}{h}\right)^2 + \cdots + \in^{(L)}\left(\frac{r}{h}\right)^L, \\ \rho(r) &= \rho^{(0)} + \rho^{(1)}\left(\frac{r}{h}\right)^1 + \rho^{(2)}\left(\frac{r}{h}\right)^2 + \cdots + \rho^{(L)}\left(\frac{r}{h}\right)^L. \end{aligned}$$

With implicit summation over repeated indices, $C(r)$ and $\rho(r)$ can be written compactly as

$$C(r)=C^{(l)}\left(\frac{r}{h}\right)^l,\ e(r)=e^{(l)}\left(\frac{r}{h}\right)^l,\ \in(r)=\in^{(l)}\left(\frac{r}{h}\right)^l,\ \rho(r)=\rho^{(l)}\left(\frac{r}{h}\right)^l \quad l=0,1,2\ldots,L, \tag{4}$$

where l, $C^{(l)}$ et al. are the order number and coefficients to be determined in order to fit the polynomials (4) to the original material constants of the elastic medium inside the material. In the homogeneous case, $C(r)=C^{(0)}$, $C^{(l)}=0$ $(l>0)$.

Considering the boundary of the material of the open circuit surface, the position dependence of the elastic, dielectric, piezoelectric constants and mass density is given by

$$\bar{C}(r)=C(r)\pi(r),\quad \bar{e}(r)=e(r)\pi(r),\quad \bar{\in}(r)=\in(r)\pi(r),\quad \bar{\rho}(r)=\rho(r)\pi(r), \tag{5}$$

where $\pi(r)$ is the rectangular window function defined by

$$\pi(r)=\begin{cases}1, & a\le r\le b\\ 0, & \text{elsewhere}\end{cases}.$$

Given Eqs. (5), the material constants vanish outside the material. We thus describe the vacuum outside the material as a medium with zero acoustic impedance and zero electric displacement which ensures that $T_{rr}=T_{rz}=T_{r\theta}=0$ and $D_r=0$ when $r=a$, $r=b$.

For a free harmonic wave being propagated in the circumferential direction in a circular cylinder of infinite length, we assume the displacement components and electric potential to be of the form

$$u_r(r,\theta,z,t)=\exp(ikb\theta-i\omega t)U(r), \tag{6.1}$$

$$u_\theta(r,\theta,z,t)=\exp(ikb\theta-i\omega t)V(r), \tag{6.2}$$

$$u_z(r,\theta,z,t)=\exp(ikb\theta-i\omega t)W(r), \tag{6.3}$$

$$\Phi(r,\theta,z,t)=\exp(ikb\theta-i\omega t)X(r). \tag{6.4}$$

$U(r)$, $V(r)$, $W(r)$ represent the amplitude of vibration in the radial and the two tangential directions, respectively, and $X(r)$ represents the amplitude of the electric potential. k is the magnitude of the wave vector in the propagation direction, and ω is the angular frequency.

Substituting Eqs. (1), (2), (4), (5), (6) into Eqs. (3), the governing differential equations in terms of the displacement components and electric potential can be obtained:

$$\begin{aligned}
&\frac{1}{h^l}\{r^{l+2}\left(C_{33}^{(l)}U''+C_{35}^{(l)}V''+C_{34}^{(l)}W''+e_{33}^{(l)}X''\right)+r^{l+1}\Big[\left((l+1)C_{33}^{(l)}+2ikbC_{35}^{(l)}\right)U'\\
&+\left(lC_{35}^{(l)}-C_{15}^{(l)}\right)V'+ikb\left(C_{13}^{(l)}+C_{55}^{(l)}\right)V'+\left((l+1)C_{34}^{(l)}-C_{14}^{(l)}\right)W'+ikb\left(C_{36}^{(l)}+C_{45}^{(l)}\right)W'\\
&+\left((l+1)e_{33}^{(l)}-e_{31}^{(l)}+ikb\left(e_{13}^{(l)}+e_{35}^{(l)}\right)\right)X'\Big]+r^l\Big[l\left(C_{13}^{(l)}+ikbC_{35}^{(l)}\right)U-\left(C_{11}^{(l)}+k^2b^2C_{55}^{(l)}\right)U\\
&+l\left(ikbC_{13}^{(l)}-C_{35}^{(l)}\right)V+\left(C_{15}^{(l)}-k^2b^2C_{15}^{(l)}-ikb\left(C_{11}^{(l)}+C_{55}^{(l)}\right)\right)V\\
&+\left(ikb\left(lC_{36}^{(l)}-C_{16}^{(l)}\right)-k^2b^2C_{56}^{(l)}\right)W+\left((l+1)ikbe_{13}^{(l)}-ikbe_{11}^{(l)}-k^2b^2e_{15}^{(l)}\right)X\Big]\pi(r)\\
&+(\delta(r-a)-\delta(r-b))\frac{1}{h^l}\{r^{l+2}\left(C_{33}^{(l)}U'+C_{35}^{(l)}V'+C_{34}^{(l)}W'+e_{33}^{(l)}X'\right)\\
&+r^{l+1}\Big[\left(C_{13}^{(l)}+ikbC_{35}^{(l)}\right)U+\left(ikbC_{13}^{(l)}-C_{35}^{(l)}\right)V+ikbC_{36}^{(l)}W+ikbe_{13}^{(l)}X\Big]\Big\}\\
&=-\frac{\rho^{(l)}r^{l+2}\omega^2}{h^l}U\pi(r),
\end{aligned} \tag{7.1}$$

$$\frac{1}{h^l}\Big\{r^{l+2}\Big(C_{35}^{(l)}U''+C_{55}^{(l)}V''+C_{45}^{(l)}W''+e_{35}^{(l)}X''\Big)$$
$$+r^{l+1}\Big[\Big((l+2)C_{35}^{(l)}+C_{15}^{(l)}+ikb\Big(C_{13}^{(l)}+C_{55}^{(l)}\Big)\Big)U'+\Big((l+1)C_{55}^{(l)}+2ikbC_{15}^{(l)}\Big)V'+(l+2)C_{45}^{(l)}W'$$
$$+ikb\Big(C_{14}^{(l)}+C_{56}^{(l)}\Big)W'+ikb\Big(e_{31}^{(l)}+e_{15}^{(l)}\Big)X'+(l+2)e_{35}^{(l)}X'\Big]+r^{l}\Big[(l+1)\Big(C_{15}^{(l)}+ikbC_{55}^{(l)}\Big)U$$
$$+\Big(ikbC_{11}^{(l)}-k^2b^2C_{15}^{(l)}\Big)U+\Big(likbC_{15}^{(l)}-(l+1)C_{55}^{(l)}-k^2b^2C_{11}^{(l)}\Big)V$$
$$\times\Big((l+1)ikbC_{56}^{(l)}-k^2b^2C_{16}^{(l)}\Big)W+(l+2)ikbe_{15}^{(l)}X-k^2b^2e_{11}^{(l)}X\Big]\Big\}\pi(r)$$
$$+(\delta(r-a)-\delta(r-b))\frac{1}{h^l}\big\{r^{l+2}\Big(C_{35}^{(l)}U'+C_{55}^{(l)}V'+C_{45}^{(l)}W'+e_{35}^{(l)}X'\Big)$$
$$+r^{l+1}\Big[\Big(C_{15}^{(l)}+ikbC_{55}^{(l)}\Big)\Big)U+\Big(ikbC_{15}^{(l)}-C_{55}^{(l)}\Big)V+ikbC_{56}^{(l)}W+ikbe_{15}^{(l)}X\Big]\Big\}$$
$$=-\frac{\rho^{(l)}r^{l+2}\omega^2}{h^l}V\pi(r), \tag{7.2}$$

$$\frac{1}{h^l}\Big\{r^{l+2}\Big(C_{34}^{(l)}U''+C_{45}^{(l)}V''+C_{44}^{(l)}W''+e_{34}^{(l)}X''\Big)+r^{l+1}\Big[\Big((l+1)C_{34}^{(l)}+C_{14}^{(l)}+ikb\Big(C_{36}^{(l)}+C_{45}^{(l)}\Big)\Big)U'$$
$$+\Big(lC_{45}^{(l)}+ikb\Big(C_{14}^{(l)}+C_{56}^{(l)}\Big)\Big)V'+\Big((l+1)C_{44}^{(l)}+2ikbC_{46}^{(l)}\Big)W'+\Big(ikb\Big(e_{36}^{(l)}+e_{14}^{(l)}\Big)+(l+1)e_{34}^{(l)}\Big)X'\Big]$$
$$+r^{l}\Big(l\Big(C_{14}^{(l)}+ikbC_{45}^{(l)}\Big)+ikbC_{16}^{(l)}-k^2b^2C_{56}^{(l)}\Big)U+\Big(l\Big(ikbC_{14}^{(l)}-C_{45}^{(l)}\Big)-ikbC_{56}^{(l)}-k^2b^2C_{16}^{(l)}\Big)V$$
$$+\Big(likbC_{46}^{(l)}-k^2b^2C_{66}^{(l)}\Big)W+\Big((l+1)ikbe_{14}^{(l)}-k^2b^2e_{16}^{(l)}\Big)X\Big]\Big\}\pi(r)+(\delta(r-a)-\delta(r-b))\frac{1}{h^l}$$
$$\times\big\{r^{l+2}\Big(C_{34}^{(l)}U'+C_{45}^{(l)}V'+C_{44}^{(l)}W'+e_{34}^{(l)}X'\Big)+r^{l+1}\Big[\Big(C_{14}^{(l)}+ikbC_{45}^{(l)}\Big)U+\Big(ikbC_{14}^{(l)}-C_{45}^{(l)}\Big)V$$
$$+ikbC_{46}^{(l)}W+ikbe_{14}^{(l)}X\Big]\Big\}=-\frac{\rho^{(l)}r^{l+2}\omega^2}{h^l}W\pi(r), \tag{7.3}$$

$$\frac{1}{h^l}\big\{r^{l+2}\Big(e_{33}^{(l)}U''+e_{35}^{(l)}V''+e_{34}^{(l)}W''-\in_{33}^{(l)}X''\Big)+r^{l+1}\Big[\Big(e_{31}^{(l)}+(l+1)e_{33}^{(l)}+ikb\Big(e_{13}^{(l)}+e_{35}^{(l)}\Big)\Big)U'$$
$$+\Big(ikb\Big(e_{31}^{(l)}+e_{15}^{(l)}\Big)+le_{35}^{(l)}\Big)V'+\Big(ikb\Big(e_{36}^{(l)}+e_{14}^{(l)}\Big)+(l+1)e_{34}^{(l)}\Big)W'-\Big((l+1)\in_{33}^{(l)}+2ikb\in_{13}^{(l)}\Big)X'\Big]$$
$$+r^{l}\Big[\Big(l\Big(e_{31}^{(l)}+ikbe_{35}^{(l)}\Big)-k^2b^2e_{15}^{(l)}+ikbe_{11}^{(l)}\Big)U+\Big(l\Big(ikbe_{31}^{(l)}-e_{35}^{(l)}\Big)-ikbe_{15}^{(l)}-k^2b^2e_{11}\Big)V$$
$$+\Big(likbe_{36}^{(l)}-k^2b^2e_{16}^{(l)}\Big)W-\Big((l+1)ikb\in_{13}^{(l)}-k^2b^2\in_{11}^{(l)}\Big)X\Big]\Big\}\pi(r)$$
$$+(\delta(r-a)-\delta(r-b))\frac{1}{h^l}\big\{r^{l+2}\Big(e_{33}^{(l)}U'+e_{35}^{(l)}V'+e_{34}^{(l)}W'-\in_{33}^{(l)}X'\Big)$$
$$+r^{l+1}\Big[\Big(e_{31}^{(l)}+ikbe_{35}^{(l)}\Big)U+\Big(ikbe_{31}^{(l)}-e_{35}^{(l)}\Big)V+ikbe_{36}^{(l)}W-ikb\in_{13}^{(l)}X\Big]\Big\}=0, \tag{7.4}$$

where, $U(r)$, $V(r)$, $W(r)$ and $X(r)$ can be expanded to Legendre orthogonal polynomial series as

$$U(r)=\sum_{m=0}^{\infty}p_m^1Q_m(r),\quad V(r)=\sum_{m=0}^{\infty}p_m^2Q_m(r),\quad W(r)=\sum_{m=0}^{\infty}p_m^3Q_m(r),\quad X(r)=\sum_{m=0}^{\infty}r_mQ_m(r), \tag{8}$$

where p_m^i ($i=1, 2, 3$) and r_m are the expansion coefficients and

$$Q_m(r) = \sqrt{\frac{2m+1}{(b-a)}} P_m\left(\frac{2r-(b+a)}{(b-a)}\right)$$

with P_m is the mth Legendre polynomial. Theoretically, m runs from 0 to ∞. In practice, the summation over the polynomials in Eqs. (8) can be stopped at some finite value $m = M$, when higher order terms become essentially negligible.

Multiplying by $Q^*_j(r)$ with j running from 0 to M, integrating over r from a to b, and taking advantage of the orthonormality of the functions $Q_m(r)$ gives the following systems

$$A_{11}^{j,m} p_m^1 + A_{12}^{j,m} p_m^2 + A_{13}^{j,m} p_m^3 + A_{14}^{j,m} r_m = -\omega^2 M_m^j p_m^1, \tag{9.1}$$

$$A_{21}^{j,m} p_m^1 + A_{22}^{j,m} p_m^2 + A_{23}^{j,m} p_m^3 + A_{24}^{j,m} r_m = -\omega^2 M_m^j p_m^2, \tag{9.2}$$

$$A_{31}^{j,m} p_m^1 + A_{32}^{j,m} p_m^2 + A_{33}^{j,m} p_m^3 + A_{34}^{j,m} r_m = -\omega^2 M_m^j p_m^3, \tag{9.3}$$

$$A_{41}^{j,m} p_m^1 + A_{42}^{j,m} p_m^2 + A_{43}^{j,m} p_m^3 + A_{44}^{j,m} r_m = 0, \tag{9.4}$$

where $A_{\alpha\beta}^{j,m}$ (α, $\beta = 1, 2, 3, 4$) and M_m^j are the elements of a non-symmetric matrix. They can be obtained according to Eqs. (7).

Equation (9.4) can be written as

$$r_m = -\left(A_{44}^{j,m}\right)^{-1}\left(A_{41}^{j,m} p_m^1 + A_{42}^{j,m} p_m^2 + A_{43}^{j,m} p_m^3\right). \tag{10}$$

Substituting Eq. (10) into Eqs. (9.1), (9.2) and (9.3):

$$\begin{aligned}&\left[A_{11}^{j,m} - A_{14}^{j,m}\left(A_{44}^{j,m}\right)^{-1} A_{41}^{j,m}\right] p_m^1 + \left[A_{12}^{j,m} - A_{14}^{j,m}\left(A_{44}^{j,m}\right)^{-1} A_{42}^{j,m}\right] p_m^2 \\ &\quad + \left[A_{13}^{j,m} - A_{14}^{j,m}\left(A_{44}^{j,m}\right)^{-1} A_{43}^{j,m}\right] p_m^3 = -\omega^2 M_m^j p_m^1,\end{aligned} \tag{11.1}$$

$$\begin{aligned}&\left[A_{21}^{j,m} - A_{24}^{j,m}\left(A_{44}^{j,m}\right)^{-1} A_{41}^{j,m}\right] p_m^1 + \left[A_{22}^{j,m} - A_{24}^{j,m}\left(A_{44}^{j,m}\right)^{-1} A_{42}^{j,m}\right] p_m^2 \\ &\quad + \left[A_{23}^{j,m} - A_{24}^{j,m}\left(A_{44}^{j,m}\right)^{-1} A_{43}^{j,m}\right] p_m^3 = -\omega^2 M_m^j p_m^2,\end{aligned} \tag{11.2}$$

$$\begin{aligned}&\left[A_{31}^{j,m} - A_{34}^{j,m}\left(A_{44}^{j,m}\right)^{-1} A_{41}^{j,m}\right] p_m^1 + \left[A_{32}^{j,m} - A_{34}^{j,m}\left(A_{44}^{j,m}\right)^{-1} A_{42}^{j,m}\right] p_m^2 \\ &\quad + \left[A_{33}^{j,m} - A_{34}^{j,m}\left(A_{44}^{j,m}\right)^{-1} A_{42}^{j,m}\right] p_m^3 = -\omega^2 M_m^j p_m^3.\end{aligned} \tag{11.3}$$

Equations (11) can be written as

$$\begin{bmatrix} \bar{A}_{11}^{j,m} & \bar{A}_{12}^{j,m} & \bar{A}_{13}^{j,m} \\ \bar{A}_{21}^{j,m} & \bar{A}_{22}^{j,m} & \bar{A}_{22}^{j,m} \\ \bar{A}_{31}^{j,m} & \bar{A}_{32}^{j,m} & \bar{A}_{33}^{j,m} \end{bmatrix} \begin{Bmatrix} p_m^1 \\ p_m^2 \\ p_m^3 \end{Bmatrix} = -\omega^2 \begin{bmatrix} M_m^j & 0 & 0 \\ 0 & M_m^j & 0 \\ 0 & 0 & M_m^j \end{bmatrix} \begin{Bmatrix} p_m^1 \\ p_m^2 \\ p_m^3 \end{Bmatrix}. \tag{12}$$

So, Eqs. (12) yield a form of the eigenvalue problem. The eigenvalue ω^2 gives the angular frequency of the guided wave; the eigenvectors p_m^i ($i = 1, 2, 3$) allow the components of the particle displacement to be calculated; and r_m, which can be obtained according to Eq. (10), determines the electric potential distribution. Using $Vph = \omega/k$ and $Vg = d\omega/dk$, the phase velocity and group velocity can be obtained. The complex matrix Eq. (12) can be solved numerically making use of standard computer programs for the diagonalization of non-symmetric square matrices. In practice

the summations over the polynomials in the $3(M+1)$ eigenmodes are generated from the order M of the expansion. Acceptable solutions are those eigenmodes for which convergence is obtained as M is increased. We assume that the eigenvalues obtained are converged solutions when a further increase in the matrix dimension does not result in a significant change in the eigenvalue. The computer program was written using Mathmatica.

When the material is orthotropic or has fewer independent constants in the wave propagation direction and is polarized in the radial direction, the governing differential equations are reduced to

$$\begin{aligned}
&\frac{1}{h^l}\Big\{r^{l+2}\Big(C_{33}^{(l)}U''+e_{33}^{(l)}X''\Big)+r^{l+1}\Big[(l+1)C_{33}^{(l)}U'+ikb\Big(C_{13}^{(l)}+C_{55}^{(l)}\Big)V'+\Big((l+1)e_{33}^{(l)}-e_{31}^{(l)}\Big)X'\Big]\\
&\quad+r^l\Big[lC_{13}^{(l)}U-\Big(C_{11}^{(l)}+k^2b^2C_{55}^{(l)}\Big)U+likbC_{13}^{(l)}V-ikb\Big(C_{11}^{(l)}+C_{55}^{(l)}\Big)V-k^2b^2e_{15}^{(l)}X\Big]\pi(r)\\
&\quad+(\delta(r-a)-\delta(r-b))\frac{1}{h^l}\Big[r^{l+2}\Big(C_{33}^{(l)}U'+e_{33}^{(l)}X'\Big)+r^{l+1}\Big(C_{13}^{(l)}U+ikbC_{13}^{(l)}V\Big)\Big]\\
&=-\frac{\rho^{(l)}r^{l+2}\omega^2}{h^l}U\pi(r),
\end{aligned}\tag{13.1}$$

$$\begin{aligned}
&\frac{1}{h^l}\Big\{r^{l+2}C_{55}^{(l)}V''+r^{l+1}\Big[ikb\Big(C_{13}^{(l)}+C_{55}^{(l)}\Big)U'+(l+1)C_{55}^{(l)}V'+ikb\Big(e_{31}^{(l)}+e_{15}^{(l)}\Big)X'\Big]\\
&\quad+r^l\Big[\Big(ikb(l+1)C_{55}^{(l)}+C_{11}^{(l)}\Big)U-\Big((l+1)C_{55}^{(l)}+k^2b^2C_{11}^{(l)}\Big)V+(l+2)ikbe_{15}^{(l)}X\Big]\Big\}\pi(r)\\
&\quad+(\delta(r-a)-\delta(r-b))\frac{1}{h^l}\Big[r^{l+2}C_{55}^{(l)}V'+r^{l+1}\Big(ikbC_{55}^{(l)}U-C_{55}^{(l)}V+ikbe_{15}^{(l)}X\Big)\Big]\\
&=-\frac{\rho^{(l)}r^{l+2}\omega^2}{h^l}V\pi(r),
\end{aligned}\tag{13.2}$$

$$\begin{aligned}
&\frac{1}{h^l}\Big[r^{l+2}C_{44}^{(l)}W''+r^{l+1}(l+1)C_{44}^{(l)}W'-r^lk^2b^2C_{66}^{(l)}W\Big]\pi(r)\\
&\quad+(\delta(r-a)-\delta(r-b))\frac{1}{h^l}r^{l+2}C_{44}^{(l)}W'=-\frac{\rho^{(l)}r^{l+2}\omega^2}{h^l}W\pi(r),
\end{aligned}\tag{13.3}$$

$$\begin{aligned}
&\frac{1}{h^l}\Big\{r^{l+2}\Big(e_{33}^{(l)}U''-\in_{33}^{(l)}X''\Big)+r^{l+1}\Big[\Big(e_{31}^{(l)}+(l+1)e_{33}^{(l)}\Big)U'+ikb\Big(e_{31}^{(l)}+e_{15}^{(l)}\Big)V'-(l+1)\in_{33}^{(l)}X'\Big]\\
&\quad+r^l\Big[\Big(le_{31}^{(l)}-k^2b^2e_{15}^{(l)}\Big)U+ikb\Big(le_{31}^{(l)}-e_{15}^{(l)}\Big)V+k^2b^2\in_{11}^{(l)}X\Big]\Big\}\pi(r)\\
&\quad+(\delta(r-a)-\delta(r-b))\frac{1}{h^l}\Big[r^{l+2}\Big(e_{33}^{(l)}U'-\in_{33}^{(l)}X'\Big)+r^{l+1}(U+ikbV)e_{31}^{(l)}\Big]=0.
\end{aligned}\tag{13.4}$$

Here, Eq. (13.3) is independent of the other three equations, and Eqs. (13.1), (13.2), (13.4) are coupled with each other. In fact, Eq. (13.3) represents the propagating circumferential SH wave. It is not influenced by the piezoelectricity when the material is polarized in the radial direction, and it can be solved analytically. Equations (13.1) and (13.2) control the propagating Lamb-like wave.

When the material is orthotropic and is polarized in the circumferential direction, the governing differential equations are

$$\begin{aligned}
&\frac{1}{h^l}\Big\{r^{l+2}C_{33}^{(l)}U''+r^{l+1}\Big[(l+1)C_{33}^{(l)}U'+ikb\Big(C_{13}^{(l)}+C_{55}^{(l)}\Big)V'+ikbe_{35}^{(l)}X'\Big]\\
&\quad+r^l\Big[lC_{13}^{(l)}U-\Big(C_{11}^{(l)}+k^2b^2C_{55}^{(l)}\Big)U+likbC_{13}^{(l)}V-ikb\Big(C_{11}^{(l)}+C_{55}^{(l)}\Big)V+ikb\Big((l+1)e_{13}^{(l)}-e_{11}^{(l)}\Big)X\Big]\pi(r)\\
&\quad+(\delta(r-a)-\delta(r-b))\frac{1}{h^l}\Big[r^{l+2}C_{33}^{(l)}U'+r^{l+1}\Big(C_{13}^{(l)}U+ikbC_{13}^{(l)}V+ikbe_{13}^{(l)}X\Big)\Big]\\
&=-\frac{\rho^{(l)}r^{l+2}\omega^2}{h^l}U\pi(r),
\end{aligned}\tag{14.1}$$

$$\frac{1}{h^l}\Big\{r^{l+2}\Big(C_{55}^{(l)}V''+e_{35}^{(l)}X''\Big)+r^{l+1}\Big[ikb\Big(C_{13}^{(l)}+C_{55}^{(l)}\Big)U'+(l+1)C_{55}^{(l)}V'+(l+2)e_{35}^{(l)}X'\Big]$$
$$+r^{l}\Big[\Big(ikb(l+1)C_{55}^{(l)}+C_{11}^{(l)}\Big)U-\Big((l+1)C_{55}^{(l)}+k^2b^2C_{11}^{(l)}\Big)V-k^2b^2e_{11}^{(l)}X\Big]\Big\}\pi(r)$$
$$+(\delta(r-a)-\delta(r-b))\frac{1}{h^l}\Big[r^{l+2}\Big(C_{55}^{(l)}V'+e_{35}^{(l)}X'\Big)+r^{l+1}\Big(ikbC_{55}^{(l)}U-C_{55}^{(l)}V\Big)\Big]$$
$$=-\frac{\rho^{(l)}r^{l+2}\omega^2}{h^l}V\pi(r), \tag{14.2}$$

$$\frac{1}{h^l}\Big[r^{l+2}C_{44}^{(l)}W''+r^{l+1}(l+1)C_{44}^{(l)}W'-r^lk^2b^2C_{66}^{(l)}W\Big]\pi(r)$$
$$+(\delta(r-a)-\delta(r-b))\frac{1}{h^l}r^{l+2}C_{44}^{(l)}W'=-\frac{\rho^{(l)}r^{l+2}\omega^2}{h^l}W\pi(r), \tag{14.3}$$

$$\frac{1}{h^l}\{r^{l+2}\Big(e_{35}^{(l)}V''-\in_{33}^{(l)}X''\Big)+r^{l+1}\Big[ikb\Big(e_{13}^{(l)}+e_{35}^{(l)}\Big)U'+le_{35}^{(l)}V'-(l+1)\in_{33}^{(l)}X'\Big]$$
$$+r^{l}\Big[ikb\Big(le_{35}^{(l)}+e_{11}^{(l)}\Big)U-\Big(le_{35}^{(l)}+k^2b^2e_{11})V+k^2b^2\in_{11}^{(l)}\Big)X\Big]\Big\}\pi(r)$$
$$+(\delta(r-a)-\delta(r-b))\frac{1}{h^l}\Big[r^{l+2}\Big(e_{35}^{(l)}V'-\in_{33}^{(l)}X'\Big)+r^{l+1}\Big(ikbe_{35}^{(l)}U-e_{35}^{(l)}V\Big)\Big]=0 \tag{14.4}$$

Similarly, the independent SH wave is not affected by the piezoelectricity.

When the material is orthotropic and is polarized in the axial direction, the governing differential equations are

$$\frac{1}{h^l}\{r^{l+2}C_{33}^{(l)}U''+r^{l+1}\Big[(l+1)C_{33}^{(l)}U'+ikb\Big(C_{13}^{(l)}+C_{55}^{(l)}\Big)V'\Big]$$
$$+r^{l}\Big[lC_{13}^{(l)}U-\Big(C_{11}^{(l)}+k^2b^2C_{55}^{(l)}\Big)U+likbC_{13}^{(l)}V-ikb\Big(C_{11}^{(l)}+C_{55}^{(l)}\Big)V\Big]\pi(r)$$
$$+(\delta(r-a)-\delta(r-b))\frac{1}{h^l}\Big[r^{l+2}C_{33}^{(l)}U'+r^{l+1}\Big(C_{13}^{(l)}U+ikbC_{13}^{(l)}V\Big)\Big]$$
$$=-\frac{\rho^{(l)}r^{l+2}\omega^2}{h^l}U\pi(r), \tag{15.1}$$

$$\frac{1}{h^l}\Big\{r^{l+2}C_{55}^{(l)}V''+r^{l+1}\Big[ikb\Big(C_{13}^{(l)}+C_{55}^{(l)}\Big)U'+(l+1)C_{55}^{(l)}V'\Big]$$
$$+r^{l}\Big[\Big(ikb(l+1)C_{55}^{(l)}+C_{11}^{(l)}\Big)U-\Big((l+1)C_{55}^{(l)}+k^2b^2C_{11}^{(l)}\Big)V\Big]\Big\}\pi(r)$$
$$+(\delta(r-a)-\delta(r-b))\frac{1}{h^l}\Big[r^{l+2}C_{55}^{(l)}V'+r^{l+1}\Big(ikbC_{55}^{(l)}U-C_{55}^{(l)}V\Big)\Big]$$
$$=-\frac{\rho^{(l)}r^{l+2}\omega^2}{h^l}V\pi(r), \tag{15.2}$$

$$\frac{1}{h^l}\Big\{r^{l+2}\Big(C_{44}^{(l)}W''+e_{34}^{(l)}X''\Big)+r^{l+1}\Big[(l+1)C_{44}^{(l)}W'+(l+1)e_{34}^{(l)}X'\Big]-r^lk^2b^2\Big(C_{66}^{(l)}W+e_{16}^{(l)}X\Big)\Big\}\pi(r)$$
$$+(\delta(r-a)-\delta(r-b))\frac{1}{h^l}\Big[r^{l+2}\Big(C_{44}^{(l)}W'+e_{34}^{(l)}X'\Big)+r^{l+1}ikbC_{46}^{(l)}W\Big]$$
$$=-\frac{\rho^{(l)}r^{l+2}\omega^2}{h^l}W\pi(r), \tag{15.3}$$

$$\frac{1}{h^l}\{r^{l+2}\Big(e_{34}^{(l)}W''-\in_{33}^{(l)}X''\Big)+r^{l+1}\Big[(l+1)e_{34}^{(l)}W'-(l+1)\in_{33}^{(l)}X'\Big]$$
$$-r^lk^2b^2\Big(e_{16}^{(l)}W-\in_{11}^{(l)}X\Big)\Big\}\pi(r)+(\delta(r-a)-\delta(r-b))\frac{1}{h^l}r^{l+2}\Big(e_{34}^{(l)}W'-\in_{33}^{(l)}X'\Big)=0. \tag{15.4}$$

Here, only the independent circumferential SH wave is influenced by the piezoelectricity.

3 Numerical results

Based on the foregoing formulations, a computer program has been written to calculate the dispersion behavior. To calculate the effective FGPM property of two combined materials, the Voigt-type model is used here. It is expressed as

$$P(r) = P_1 V_1(r) + P_2 V_2(r), \tag{16}$$

where $V_i(r)$ and P_i, respectively, denote the volume fraction of the ith material and the corresponding property of the ith material. Here, $\sum V_i(r) = 1$. So, the properties of the graded material can be expressed as

$$P(r) = P_2 + (P_1 - P_2) V_1(r). \tag{17}$$

According to Eqs. (4), the gradient field of the material volume fraction can be expressed as a power series expansion. The coefficients of the power series can be determined using the Mathematica function 'Fit'.

For example, if the gradient field is

$$V_1(r) = \left(\frac{r-a}{h}\right)^L, \quad a \le r \le b$$

then

$$C(r) = C^{(0)} + C^{(1)}\left(\frac{r}{h}\right)^1 + C^{(2)}\left(\frac{r}{h}\right)^2 + \cdots + C^{(L)}\left(\frac{r}{h}\right)^L,$$

where

$$C^{(l)} = C_2 + (C_1 - C_2)\frac{L!}{l!(L-l)!}\left(\frac{a}{h}\right)^l, \quad 0 \le l \le L.$$

In order to validate the computer program, guided waves dispersion curves in an FGPM cylindrical curved plate with large ratio of radius to thickness are calculated to compare the results with those of an FGPM flat plate of Lefebvre et al. [7]. Then graded cylindrical curved plates at different ratios of the inner radius to thickness are analyzed.

3.1 Comparison with available data

As is well known, the dispersion curves for a flat plate are almost the same as those for a hollow cylinder with large ratio of radius to thickness. In this example, a comparison is made of the results of an FGPM flat plate obtained by Lefebvre et al. [7] and the results of an FGPM cylindrical curved plate with large ratio of radius to thickness obtained using the Mathematica program. The inner surface of the cylindrical plate is $LiTaO_3$ and the ratio of inner radius to thickness is $\eta = 100$. The material constants of the inner and outer surface and the gradient field can be found in the paper of Lefebvre et al. [7]. Corresponding phase velocity dispersion curves are presented in Fig. 1. As is apparent, our results agree well with those obtained by Lefebvre. For these results, the series expansion Eqs. (8) is truncated at $M = 11$.

3.2 FGPM cylindrical curved plates

The circumferential wave behavior of the FGPM cylindrical curved plates composed of PZT-4 (inner surface) and $Ba_2NaNb_5O_{15}$ (outer surface) with $a = 9$ mm and $b = 10$ mm is calculated. In the

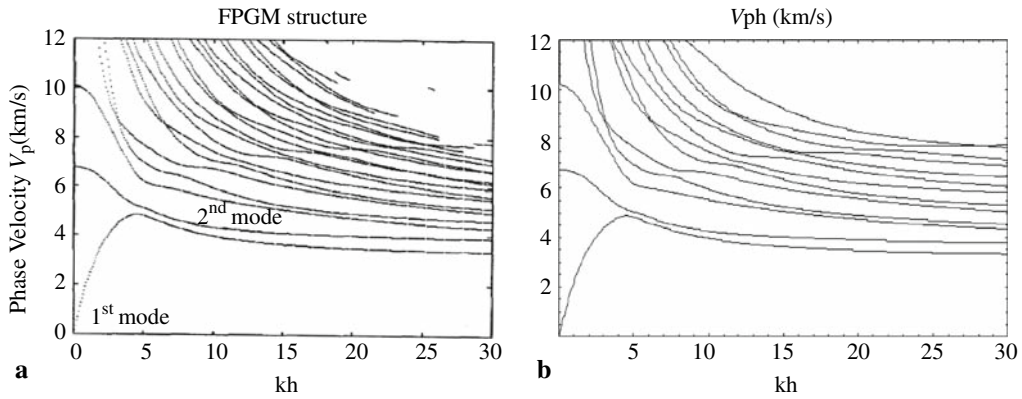

Fig. 1. **a** Dispersion curves for an FGPM plate from Lefebvre et al. [8]; **b** dispersion curves for an FGPM cylindrical curved plate when $\eta = 100$

direction of wave propagation, material constants of the two materials with radial polarization are listed in Table 1. The gradient field used here is

$$V_1(r) = \left(\frac{r-a}{h}\right)^n,$$

where n is selected as 0.5, 1, 2 and 3, respectively, i.e. four different gradient fields are considered.

Figures 2 and 3 are the frequency spectra and phase velocity spectra for the four FGPM cylindrical curved plates and the corresponding FGM cylindrical curved plates to show the piezoelectric effect. It can be seen that the effect of piezoelectricity is so strong as not to be ignored, and the phase velocity in an FGPM cylindrical curved plate is higher than in the FGM cylindrical curved plate. For a definite mode, the effect becomes stronger as the wave number increases. Furthermore, for the four FGPM cylindrical curved plates, the piezoelectric effect becomes stronger as the power n increases. In order to explain this phenomenon, Figs. 4 and 5 give the frequency spectra and phase velocity spectra for the pure PZT-4 and $Ba_2NaNb_5O_{15}$ cylindrical curved plates and their corresponding non-piezoelectric cylindrical plates. Obviously, the piezoelectric effect of a PZT-4 cylindrical plate is stronger than that of a $Ba_2NaNb_5O_{15}$ cylindrical plate. It is known from Eq. (17) that the volume fraction of PZT-4 increases as the power n increases.

The electric potential distribution of the FGPM cylindrical curved plate is investigated. Figure 6 shows the lowest nine electric potential distributions of the FGPM cylindrical curved plate of Fig. 1b when $k = 300{,}000$ rad/m. It can be seen that the electric potential in the FGPM cylindrical curved

Table 1. Material constants of two homogeneous piezoelectric materials

Property	C_{11}	C_{12}	C_{13}	C_{22}	C_{23}	C_{33}	C_{44}	C_{55}	C_{66}
$Ba_2NaNb_5O_{15}$	23.9	10.4	5	24.7	5.2	13.5	6.5	6.6	7.6
PZT-4	13.9	7.8	7.4	13.9	7.4	11.5	2.56	2.56	3.05
	e_{15}	e_{24}	e_{31}	e_{32}	e_{33}	ϵ_{11}	ϵ_{22}	ϵ_{33}	ρ
$Ba_2NaNb_5O_{15}$	2.8	3.4	−0.4	−0.3	4.3	196	201	28	5.3
PZT-4	12.7	12.7	−5.2	−5.2	15.1	650	650	560	7.5

Units: C_{ij} (10^{10} N/m^2), ϵ_{ij} (10^{-11} F/m^2), e_{ij} (C/m), ρ (kg/m^3)

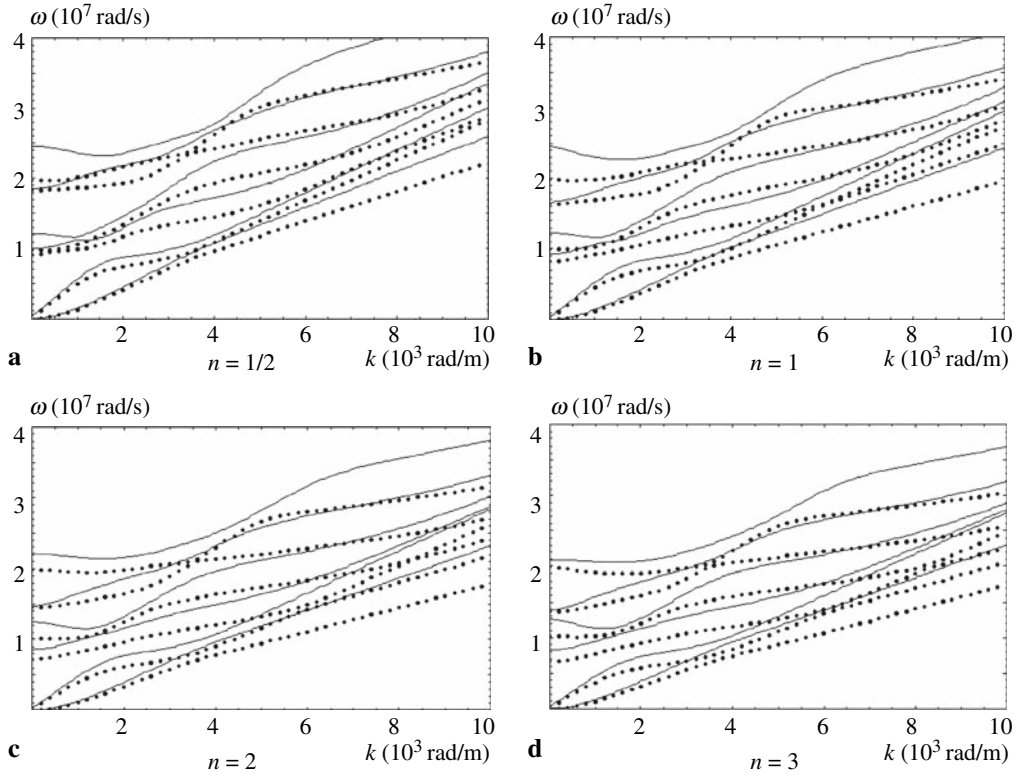

Fig. 2. Frequency spectra for a cylindrical curved plate (*dotted line* FGM, *solid line* FGPM)

plate is distributed mainly near the outer or inner surface. For the lower modes, the electric potential is distributed mainly near the inner surface. As the mode order increases, the electric potential distribution turns to the outer surface. Up to the eighth mode, the electric potential has been distributed mainly near the outer surface.

Consider a similar structure to the one in Fig. 1b, but exchange the material of outer and inner surfaces. The inner surface is $Ba_2NaNb_5O_{15}$ and the outer surface is PZT-4. The other conditions are consistent with the ones in Fig. 1b. Figure 7 is the dispersion curve for this structure. No much difference between the dispersion curves for the two structures can be found. Their piezoelectric effects are also similar. In fact, the volume fractions of the two materials in the two structures are almost equal. The electric potential distribution of this FGPM cylindrical curved plate is shown in Fig. 8. Similarly to Fig. 6, the electric potential is distributed mainly near the outer or inner surface. However, in contrast to Fig. 6, for the lower modes, the electric potential distribute mainly near the outer surface. As the mode order increases, the electric potential distribution turns to the mainly inner surface. Up to the eighth mode, the electric potential has distributed mainly near the inner surface.

3.3 Influence of ratios of the inner radius to thickness

In order to investigate the effect of η, the ratio of the outer radius to thickness, the frequency spectra and group velocity spectra for FGPM cylindrical curved plates are shown in Figs. 9 and 10, in which b is 10 and 2 mm, respectively, but keeping $h = 1$ mm unchanged, i.e. $\eta = 10$ and 2. The gradient

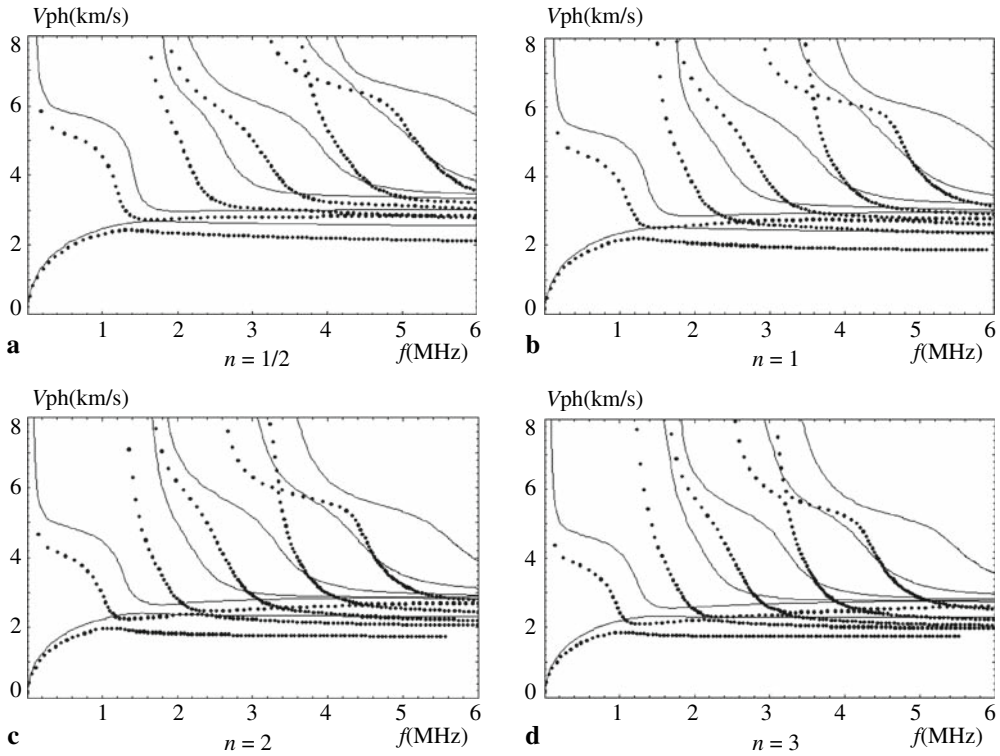

Fig. 3. Phase velocity dispersion curves for cylindrical curved plate (*dotted line* FGM, *solid line* FGPM)

field and material are the same as in the structure of Fig. 2b. From the two figures, it can be found that the ratio of radius to thickness has considerable influence on the dispersion curves for all the modes, and that the larger the wavenumber, the stronger this effect. In addition, the effect is far stronger for lower order modes than for higher order modes at smaller wavenumber. For the smaller η, the group velocity changes more sharply, and the maximum of the group velocity is larger except for the second mode. The effect of η is also obvious on the cut-off frequencies of the lower modes,

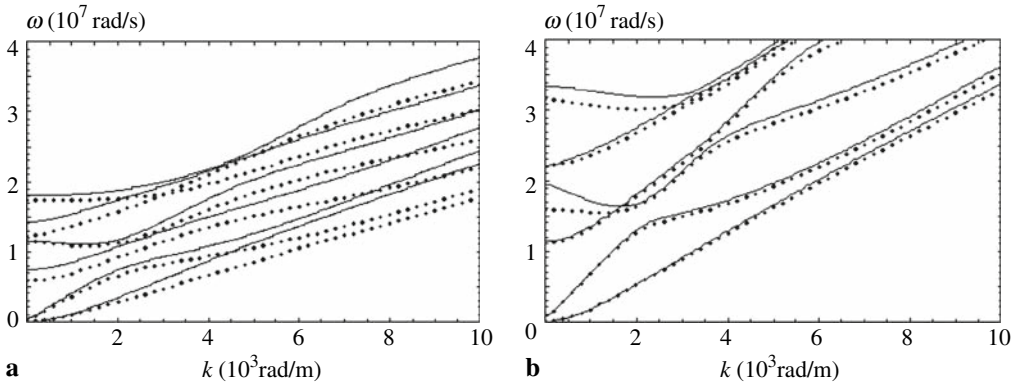

Fig. 4. Frequency spectra for PEM cylindrical curved plates: *solid line* piezoelectric, *dotted line* non-piezoelectric, **a** PZT-4; **b** $Ba_2NaNb_5O_{15}$

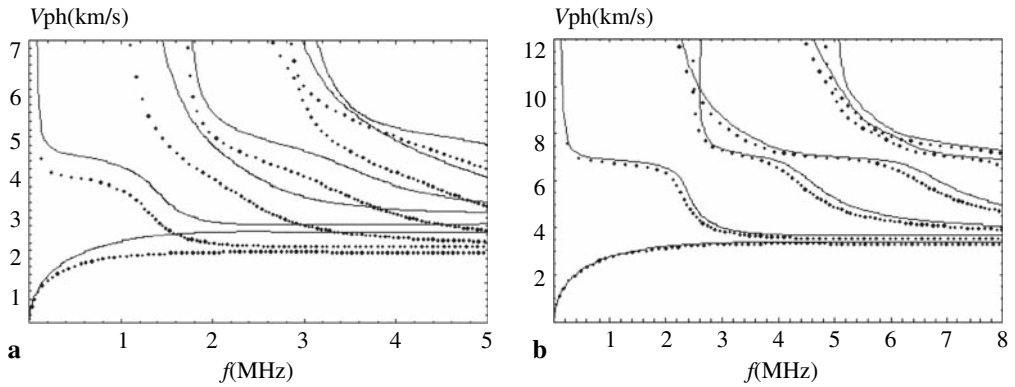

Fig. 5. Phase velocity dispersion curves for PEM cylindrical curved plates: *solid line* piezoelectric, *dotted line* non-piezoelectric; **a** PZT-4; **b** $Ba_2NaNb_5O_{15}$

especially on the first cut-off frequency. The cut-off frequencies for the smaller η are higher than for the larger η.

Figure 11 is the electric potential distribution of the FGPM cylindrical curved plate when $\eta = 2$. It is different from that of the large ratio, $\eta = 10$, in Fig. 7. For the first three modes with small ratio, the electric potential distributes mainly near the outer surface. But they distribute mainly near the inner surface for a large ratio. Figure 12 is the electric potential distribution of the FGPM cylindrical curved plate for which the inner surface is $Ba_2NaNb_5O_{15}$ and the outer surface is PZT-4 when $\eta = 2$. As known before, when the ratio is large, if the materials of inner and outer surface exchange, their

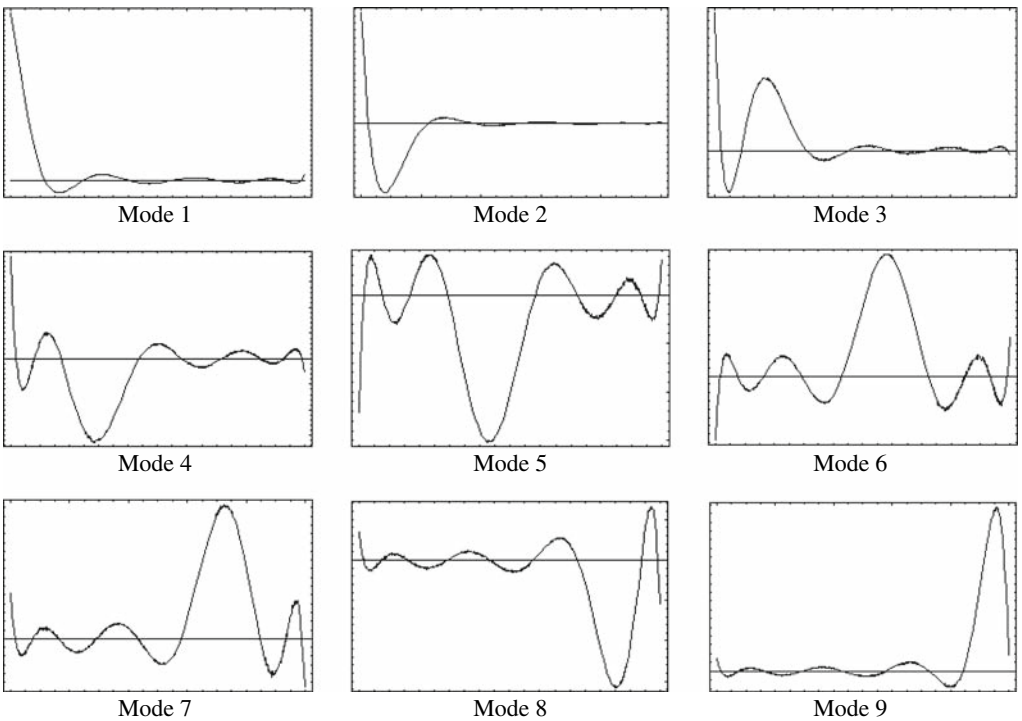

Fig. 6. Electric potential distribution in the thickness direction of the FGPM cylindrical curved plate whose inner surface is PZT-4 and outer surface is $Ba_2NaNb_5O_{15}$ ($k = 300{,}000$ rad/m)

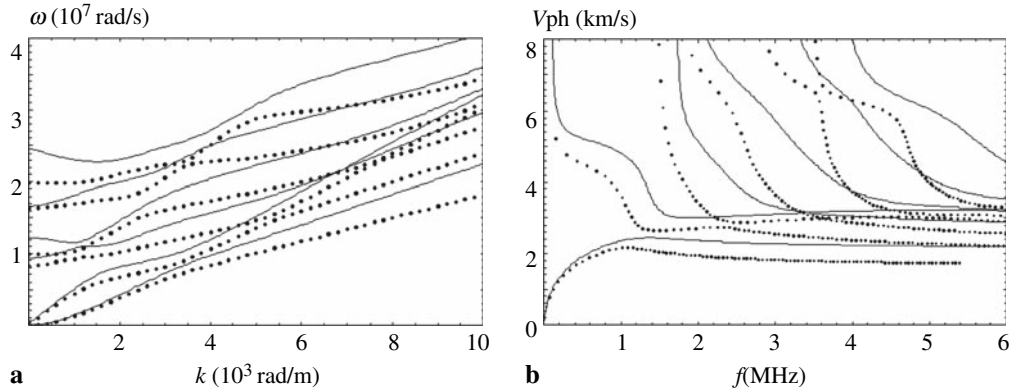

Fig. 7. Dispersion curves for cylindrical curved plate whose inner surface is $Ba_2NaNb_5O_{15}$ and outer surface is PZT-4: *solid line* FGPM, *dotted line* FGM; **a** frequency spectra, **b** phase velocity spectra

electric potential distributions are reversed. But as shown in Figs. 11 and 12, for the small ratio, whatever the inner surface is, the electric potential always distributes mainly near the outer surface for the first three modes. It is well known that the circumferential wave characteristics of large ratio hollow cylinders are very close to the wave characteristics in plates. So, for the large ratio FGPM cylindrical curved plates, the circumferential wave electric potential distributions are similar to the

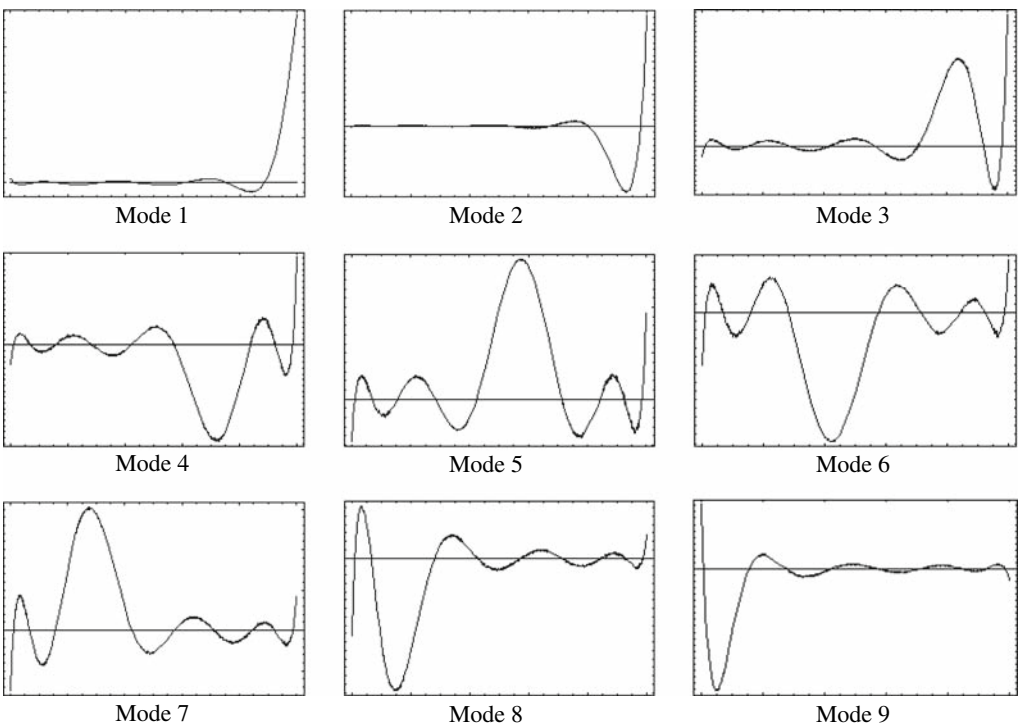

Fig. 8. Electric potential distribution in the thickness direction of FGPM cylindrical curved plate whose inner surface is $Ba_2NaNb_5O_{15}$ and outer surface is PZT-4 ($k = 300{,}000$ rad/m)

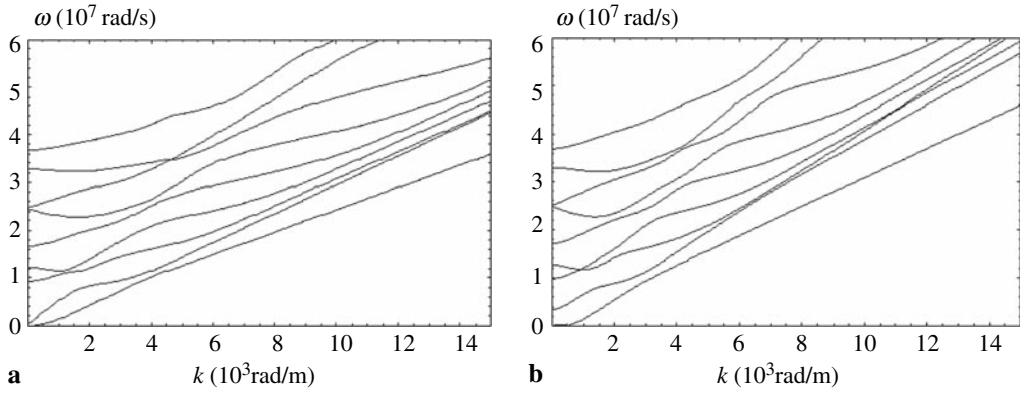

Fig. 9. Frequency dispersion curves for FGPM cylindrical curved plate, **a** $\eta = 10$, **b** $\eta = 2$

FGPM plates. But for the small ratio FGPM cylindrical curved plates, the circumferential wave electric potential distributions are different from the FGPM plate and are similar to that of the PEM cylindrical curved plate. For the PEM cylindrical curved plate, whatever the ratio is, the electric potential distributes mainly near the outer surface for the first three modes at large wave number as shown in Fig. 13. Figure 13 is the electric potential distribution of the PZT-4 cylindrical curved plate whose wall thickness is 1 mm when $\eta = 10$ and $\eta = 2$.

3.4 Influence of the polarizing direction

In this Section, the FGPM cylindrical curved plates that are polarized in circumferential and axial direction are considered. The inner radius, wall thickness, material and the gradient field are all the same to the structure of Fig. 2b. Under the circumferential and axial polarization, the dielectric and piezoelectric constants of material are listed in Table 2 and the elastic constants unchanged.

Figure 14 gives the dispersion curves for the FGPM cylindrical curved plates that are polarized in circumferential direction. It can be seen that the piezoelectric effect is stronger for the higher order modes than for lower order modes; the piezoelectric effect becomes weaker with increasing frequency and does not change considerably with varying wave number. It is different from the

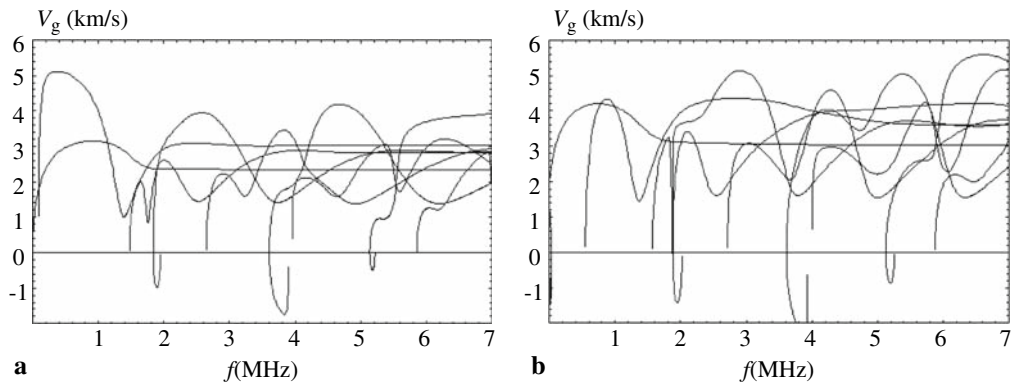

Fig. 10. Group velocity dispersion curves for FGPM cylindrical curved plate, **a** $\eta = 10$, **b** $\eta = 2$

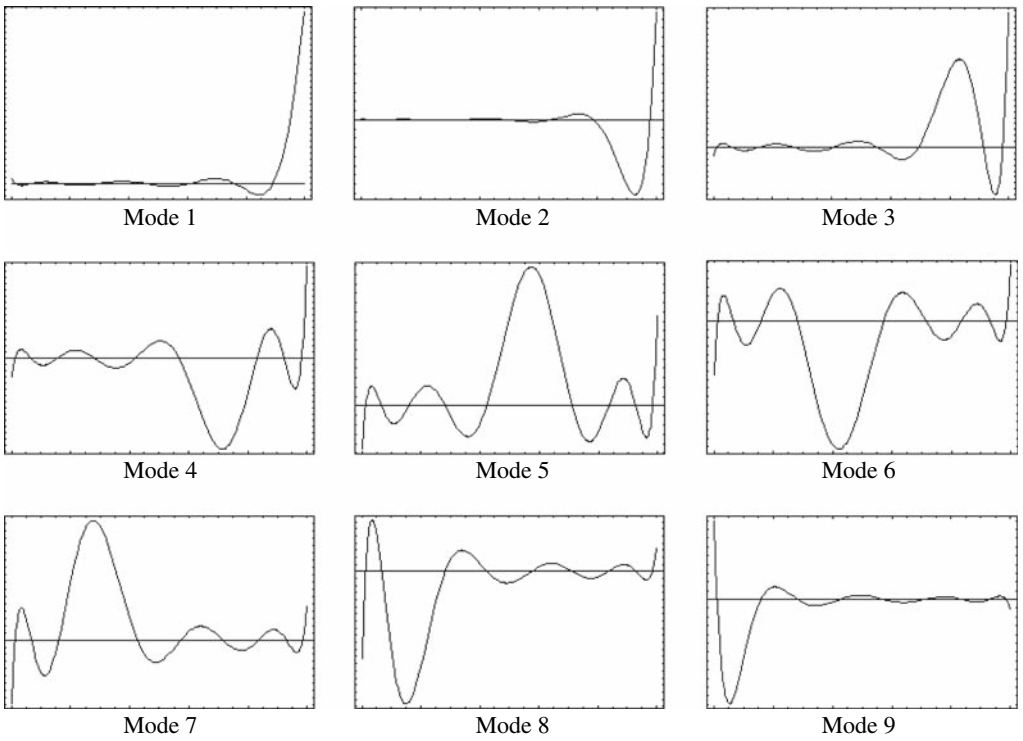

Fig. 11. Electric potential distribution in the thickness direction of an FGPM cylindrical curved plate when $\eta = 2$ whose inner surface is PZT-4 and outer surface is $Ba_2NaNb_5O_{15}$ ($k = 300{,}000$ rad/m)

radial polarization. For the radial polarization, the piezoelectric effect becomes stronger with increasing wave number and does not change obviously with the frequency varying.

For all the above cases except for the one in Fig. 1, only the circumferential Lamb-like waves are considered because the circumferential SH wave is not influenced by the piezoelectricity when the material is orthotropic and polarized in the radial or circumferential direction. Figure 15 is the circumferential SH wave dispersion curve for the FGPM cylindrical curved plates which are polarized in axial direction. This time the circumferential Lamb-like wave is not affected by the piezoelectricity. As can be seen from Fig. 15, for a definite mode, the piezoelectric effect becomes stronger with increasing wave number and does not change obviously with the frequency varying, which is similar to the radial polarization. Moreover, the piezoelectric effect is stronger on the higher order modes than on lower order modes, which is similar to the circumferential polarization. Another point should be given attention. For the first mode of the FGM cylindrical plate, the dispersion is significant, but for the FGPM cylindrical plate the dispersion is weaker. In fact, this phenomenon that piezoelectricity weakens the guided wave dispersion in the FGPM cylindrical plate can also been observed in Figs. 3 and 7b. However, for the PEM cylindrical plate, as shown in Fig. 5, the phenomenon cannot be seen.

4 Conclusions

The Legendre orthogonal polynomial series expansion method is used to characterize the guided waves in FGPM cylindrical curved plates. Guided wave dispersion curves and the electric potential

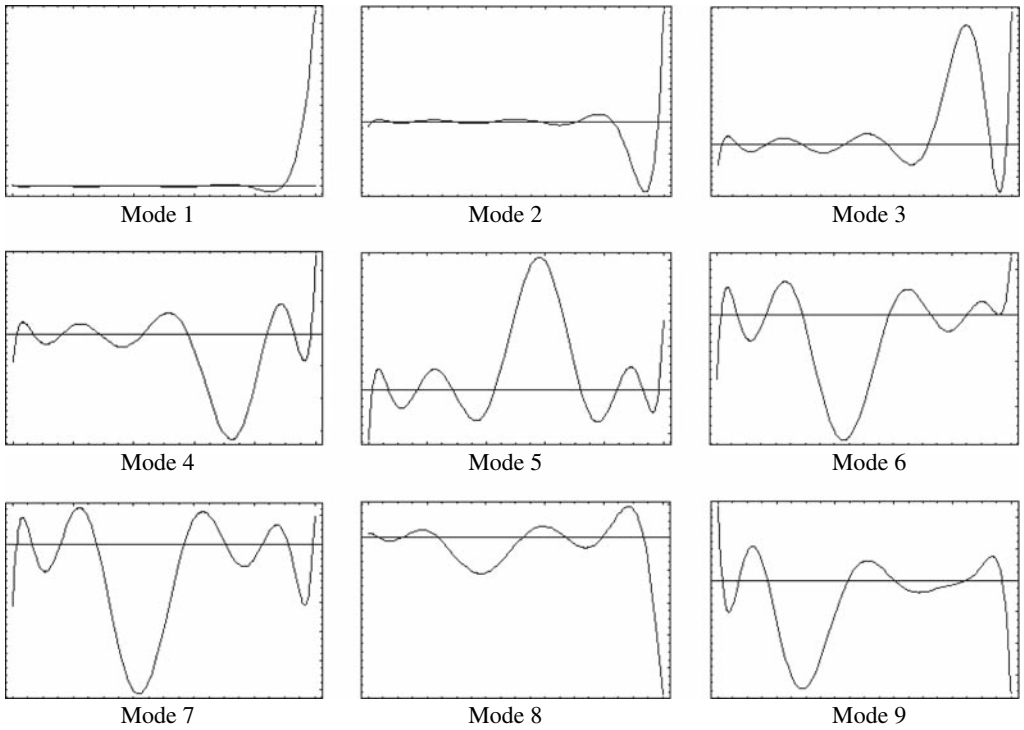

Fig. 12. Electric potential distribution in the thickness direction of an FGPM cylindrical curved plate when $\eta = 2$ whose inner surface is $Ba_2NaNb_5O_{15}$ and outer surface is PZT-4 ($k = 300{,}000$ rad/m)

distribution for FGPM cylindrical curved plates are analyzed. Based on the calculated results, the following conclusions can be drawn:

(a) For the propagating wave in FGPM cylindrical curved plates, the piezoelectric effect is considerable especially when the wave number is large.

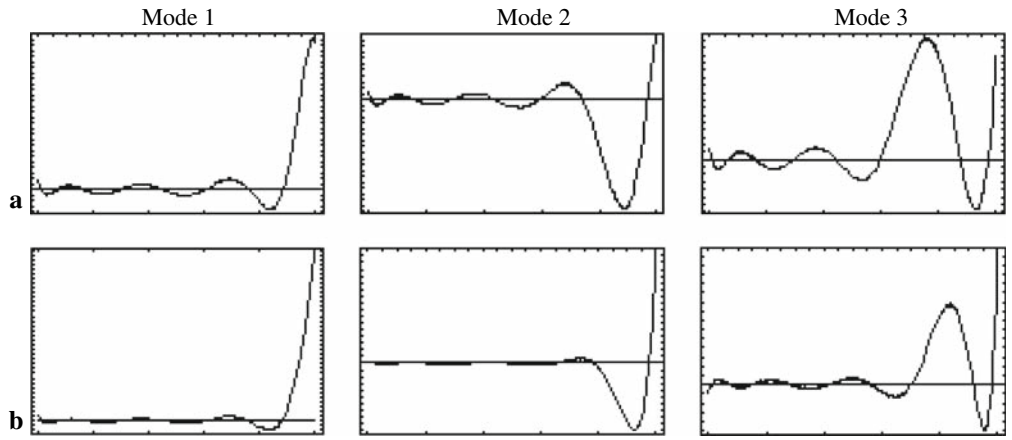

Fig. 13. Electric potential distribution in the thickness direction of PZT-4 cylindrical curved plate ($k = 300{,}000$ rad/m)

Table 2. Piezoelectric and dielectric constants of PZT-4 with axial and circumferential polarization

Polarizing direction		e_{16}	e_{21}	e_{22}	e_{23}	e_{34}	ϵ_{11}	ϵ_{22}	ϵ_{33}
Axial	PZT-4	−12.7	−15.1	5.2	5.2	−12.7	650	560	650
	$Ba_2NaNb_5O_{15}$	−3.4	0.3	−4.3	0.4	−2.8	201	28	196
		e_{11}	e_{12}	e_{13}	e_{26}	e_{35}	ϵ_{11}	ϵ_{22}	ϵ_{33}
Circumferential	PZT-4	−15.1	5.2	5.2	−12.7	−12.7	560	650	560
	$Ba_2NaNb_5O_{15}$	−4.3	0.4	0.3	−2.8	−3.4	28	196	201

Units: ϵ_{ij} (10^{-11} F/m^2), e_{ij} (C/m)

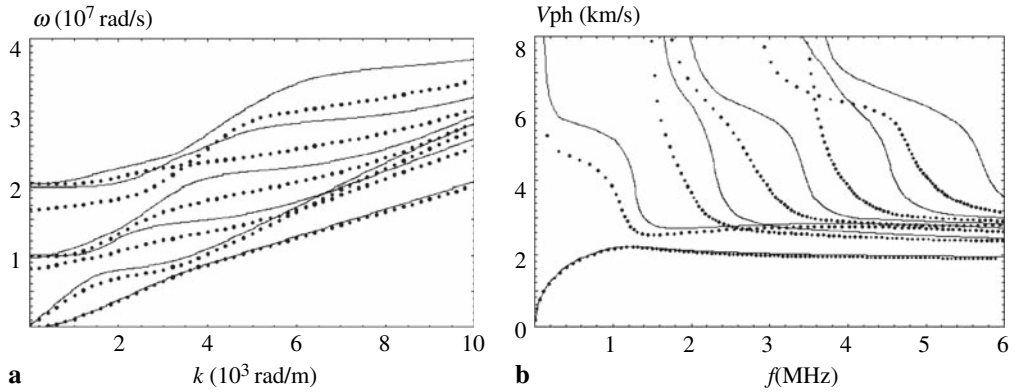

Fig. 14. Dispersion curves for a cylindrical curved plate under circumferential polarization: *solid line* FGPM, *dotted line* FGM; **a** frequency spectra, **b** phase velocity spectra

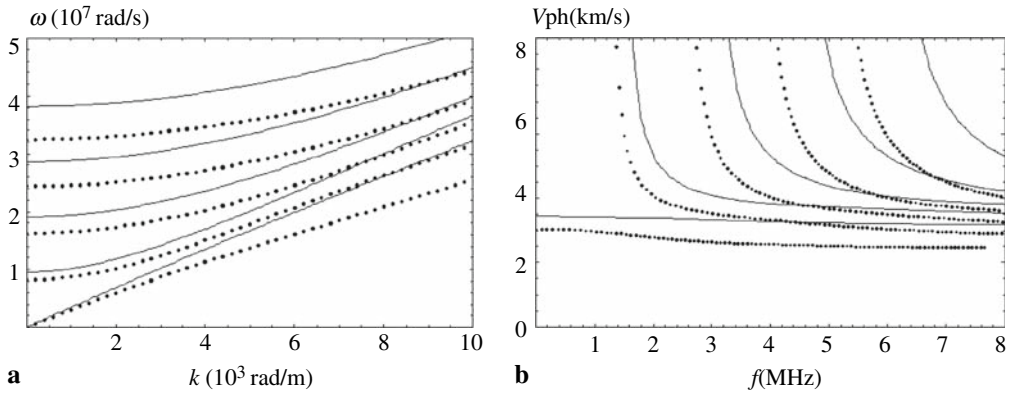

Fig. 15. Circumferential SH wave dispersion curves for cylindrical curved plate under axial polarization: *solid line* FGPM, *dotted line* FGM; **a** frequency spectra, **b** phase velocity spectra

(b) The electric potential distributes mainly near the outer or inner surface for large wave numbers.
(c) The ratio of radius to thickness has a significant influence both on the dispersion curves and on the electric potential distribution for the FGPM cylindrical curved plates.

(d) The polarizing direction can obviously change the piezoelectric effect on the dispersion curves for the FGPM cylindrical curved plates.
(e) In the FGPM cylindrical plate, piezoelectricity can weaken the guided wave dispersion.

References

[1] Kawai, T., Miyazaki, S., Araragi, M.: A new method for forming a piezoelectric FGM using a dual dispenser system. In: Yamanouchi, et al. (ed.), Proceedings of the First International Symposium on Functionally Gradient Materials, pp. 191–196. Sendai, Japan (1990)
[2] Zhu, X., Meng, Z.: Operational principle, fabrication and displacement characteristics of a functionally gradient piezoelectric ceramic actuator. Sens. Actuators A Phys. **48**, 169–176(8) (1995)
[3] Wu, C.C.M., Khan, M., Moy, W.: Piezoelectric ceramics with functional gradient: a new application of material design: a new application in material design. J. Am. Ceram. Soc. **79**, 809–812 (1996)
[4] Roy Mahapatra, D., Singhal, A., Gopalakrishnan, S.: Lamb wave characteristics of thickness-graded piezoelectric IDT. Ultrasonics **43**, 736–746 (2005)
[5] Liu, G.R., Tani, J.: Characteristics of wave propagation in functionally gradient piezoelectric material plates and its response analysis: Part 1: Theory, Part 2: Calculation results. Trans. Jpn Soc. Mech. Engng. Jpn **57(A)**, 2122–2133 (1991)
[6] Liu, G.R., Tani, J.: Surface waves in functionally gradient piezoelectric plates. Trans. Am. Soc. Mech. Engng. **116**, 440–448 (1994)
[7] Lefebvre, J.E., Zhang, V., Gazalet, J. et al.: Acoustic wave propagation in continuous functionally graded plates: an extension of the Legendre polynomial approach. IEEE Trans. Ultrason. Ferr. **48**, 1332 (2001)
[8] Han, X., Liu, G.R.: Elastic waves in a functionally graded piezoelectric cylinder. Smart Mater. Struct. **12**, 962–971 (2003)
[9] Liu, G.R., Dai, K.Y., Han, X., Ohyoshi, T.: Dispersion of waves and characteristic wave surfaces in functionally graded piezoelectric plates. J. Sound Vibr. **268**, 131–147 (2003)
[10] Chakraborty, A., Roy Mahapatra, D., Gopalakrishnan, S.: Finite element simulation of BAW propagation in inhomogeneous plate due to piezoelectric actuation. Lecture Notes in Computer Science, pp. 715–724 (2003)
[11] Chakraborty, A., Gopalakrishnan, S., Kausel, E.: Wave propagation analysis in inhomogeneous piezo-composite layer by the thin-layer method. Int. J. Numer. Methods Engng. **64**, 567–598 (2005)
[12] Li, X.Y., Wang, Z.K., Huang, S.H.: Love waves in functionally graded piezoelectric materials. Int. J. Solids Struct. **41**, 7309–7328 (2004)
[13] Liu, J., Wang, Z.K.: The propagation behavior of Love waves in a functionally graded layered piezoelectric structure. Smart Mater. Struct. **14**, 137–146 (2005)
[14] Du, J., Jin, X., Wang, J., Xian, K.: Love wave propagation in functionally graded piezoelectric material layer. Ultrasonics **46**, 13–22 (2007)
[15] Grace, O.D., Goodman, R.R.: Circumferential waves on solid cylinders. J. Acoust. Soc. Am. **39**, 173–174 (1966)
[16] Brekhovskikh, L.M.: Surface waves confined to the curvature of the boundary in solid. Sov. Phys. Acoust. **13**, 462–472 (1968)
[17] Cerv, J.: Dispersion of elastic waves and Rayleigh-type waves in a thin disc. Acta Tech. CSAV **89**, 89–99 (1988)
[18] Guo, L., Jianmin, Q.: Guided circumferential waves in a circular annulus. J. Appl. Mech. Trans. ASME **65**, 424–430 (1998)
[19] Guo, L., Jianmin, Q.: Transient wave propagation in a circular annulus subjected to transient excitation on its outer surface. J. Acoust. Soc. Am. **104**, 1210–1220 (1998)
[20] Valle, C., Qu, J., Jacobs, L.J.: Guided circumferential waves in layered cylinders. Int. J. Engng. Sci. **37**, 1369–1387 (1999)
[21] Cunfu, H., Longtao, L., Bin, W.: Guided circumferential waves in hollow cylinders. Chin. J. Mech. Engng. **40**, 7–12 (2004)

[22] Towfighi, S., Kundu, T., Ehsani, M.: Elastic wave propagation in circumferential direction in anisotropic cylindrical curved plates. J. Appl. Mech. **69**, 283–291 (2002)
[23] Jiangong, Y., Bin, W., Cunfu, H.: Guided circumferential waves in orthotropic cylindrical curved plate and the mode conversion by the end-reflection. Appl. Acoust. **68**, 594–602 (2007)
[24] Zhao, X., Rose, J.L.: Guided circumferential shear horizontal waves in an isotropic hollow cylinder. J. Acoust. Soc. Am. **115**, 1912–1916 (2004)
[25] Lefebvre, J.E., Zhang, V., Gazalet, J., Gryba, T.: Legendre polynomial approach for modeling free-ultrasonic waves in multilayered plates. J. Appl. Phys. **85**, 3419–3427 (1999)